ELSEVIER

Journal of Alloys and Compounds 216 (1994) 135–139

Journal of ALLOYS AND COMPOUNDS

Crystal chemistry of the series LnT_2B_2C (Ln = rare earth, T = transition element)

T. Siegrist, R.J. Cava, J.J. Krajewski, W.F. Peck, Jr.

AT&T Bell Laboratories, 600 Mountain Avenue, Murray Hill, NJ 07974, USA

Received 26 April 1994

Abstract

The new $LuNi_2B_2C$-type structure has been investigated for different lanthanide atoms and transition metal elements. Single-crystal structure determinations were carried out for some representative compounds, and a linear regression fit was used to infer the positional parameter of the boron atom for the whole rare earth series. In this way, detailed bonding information for all phases in the series was obtained. A geometric model, based on the conservation of bond lengths, explains the behaviour of the lattice parameters for the different size lanthanides.

1. Introduction

The new series of the quaternary intermetallic compounds based on boro-carbides show a wealth of interesting physical properties. Superconductivity at high temperature has been observed in the Y–Pd–B–C system [1], a temperature equaling the previous long-standing record of Nb_3Ge in thin-film form [2]. Superconductivity has been observed for temperatures up to 16.5 K for $LnNi_2B_2C$, where Ln are the small rare earths Lu–Ho, and Y [3], and up to 10.5 K for $LnPt_2B_2C$, where Ln = La, Pr and Y [4]. The new $LuNi_2B_2C$-type structure crystallizes in the tetragonal system, space group *I*4/*mmm*, Pearson symbol *tI*12, and they represent a new class of true quaternary intermetallics [5]. Usually, quaternary intermetallics are based on binary or ternary parent structures, with partial substitution of other elements. Only a small fraction of true ternary intermetallics showing superconductivity, like the $LuRh_4B_4$-type phases, the Chevrel phases or the $ThCr_2Si_2$ phases, have been extensively studied, and many interesting phenomena have been described. For instance, heavy fermion superconductivity in $CeCu_2Si_2$ has been observed, as well as in URu_2Si_2. In the following, we discuss the crystal chemistry of the new series of intermetallic boro-carbides, LnT_2B_2C, with Ln = lanthanide and T = transition element. A large number of phases have been prepared, and some crystal structures were investigated. Here, we present single-crystal structural data of three representatives of the $LnNi_2B_2C$ series, as well as for LaT_2B_2C with T = Rh and Ir, and extract some general bonding principles for the family.

2. Experimental details

Single-phase samples of LnT_2B_2C were obtained by arc-melting and annealing. The starting materials were lanthanide metal shavings or sublimed dendrites (99.9 to 99.99% pure), transition element powders (Ni: 99.99%, Rh:99.99%, Ir:99.9%), and coarse boron (99.6%) and carbon (99.99%) powders. Small single crystals of $LaNi_2B_2C$, $GdNi_2B_2C$ and $LuNi_2B_2C$ that were suitable for a single-crystal X-ray analysis could be obtained in this way. Powder X-ray diffraction patterns were obtained on a Phillips powder diffractometer, using copper Kα radiation. The pellets were crushed and ground, and the resulting powder was mounted on glass slides. Small thin fragments of $LaNi_2B_2C$, $GdNi_2B_2C$ and $LuNi_2B_2C$ were mounted on an Enraf–Nonius single-crystal diffractometer and diffraction intensities obtained using graphite monochromatized Mo Kα radiation. Data were collected in the $\Omega/2\Theta$-scan mode up to minimum $2\Theta = 120°$ at an ambient temperature of 23 °C. Accurate lattice parameters were obtained by determining the absolute 2Θ values at high angles of at least 35 reflections [6]. A Gaussian integration absorption correction was applied to all the intensity data measured. The structures were refined using the NRCVAX program package [7], running on a

Elsevier Science S.A.
SSDI 0925-8388(94)01260-O

SUN workstation. Crystallographic data of the three refined phases, as well as atomic positions and isotropic thermal parameters, are given in Table 1.

Table 1

Single-crystal data

$LaNi_2B_2C$

Space group *I4/mmm*, $a = 3.7941(3)$ Å, $c = 9.8224(9)$ Å, $Z = 2$, $R = 0.024$, $R_w = 0.032$ (356 independent reflections, 352 observed ($I > 2.5\ \sigma(I)$), 11 parameters)

	x	y	z	B_{iso} (Å^2)
La	0	0	0	0.429(7)
Ni	$\frac{1}{2}$	0	$\frac{1}{4}$	0.513(10)
B	0	0	0.3492(7)	0.63(9)
C	$\frac{1}{2}$	$\frac{1}{2}$	0	0.65(12)

$GdNi_2B_2C$

Space group *I/mmm*, $a = 3.5750(4)$ Å, $c = 10.3537(12)$ Å, $Z = 2$, $R = 0.042$, $R_w = 0.044$ (339 independent reflections, 337 observed ($I > 2.5\ \sigma(I)$), 11 parameters)

	x	y	z	B_{iso} (Å^2)
Gd	0	0	0	0.382(11)
Ni	$\frac{1}{2}$	0	$\frac{1}{4}$	0.428(17)
B	0	0	0.3569(12)	0.64(18)
C	$\frac{1}{2}$	$\frac{1}{2}$	0	0.38(17)

$LuNi_2B_2C$

Space group *I4/mmm*, $a = 3.4639(1)$ Å, $c = 10.6313(4)$ Å, $Z = 2$, $R = 0.025$, $R_w = 0.035$ (404 independent reflections, 387 observed ($I > 2.5\sigma(I)$), 11 parameters)

	x	y	z	B_{iso} (Å^2)
Lu	0	0	0	0.480(6)
Ni	$\frac{1}{2}$	0	$\frac{1}{4}$	0.447(10)
B	0	0	0.3618(8)	0.65(11)
C	$\frac{1}{2}$	$\frac{1}{2}$	0	0.45(10)

$LaPt_2B_2C$

Space group *I4/mmm*, $a = 3.8681(6)$ Å, $c = 10.7050(20)$ Å, $Z = 2$, $R = 0.042$, $R_w = 0.035$ (495 independent reflections, 440 observed ($I > 2.5\sigma(I)$), 11 parameters)

	x	y	z	B_{iso} (Å^2)
La	0	0	0	0.511(15)
Pt	$\frac{1}{2}$	0	$\frac{1}{4}$	0.434(10)
B	0	0	0.3617(20)	0.95(20)
C	$\frac{1}{2}$	$\frac{1}{2}$	0	0.84(22)

Table 1 (*continued*)

$LaRh_2B_2C$

Space group *I4/mmm*, $a = 3.9019(2)$ Å, $c = 10.2460(6)$ Å, $Z = 2$, $R = 0.022$, $R_w = 0.026$ (391 independent reflections, 391 observed ($I > 2.5\sigma(I)$), 11 parameters)

	x	y	z	B_{iso} (Å^2)
La	0	0	0	0.529(10)
Rh	$\frac{1}{2}$	0	$\frac{1}{4}$	0.383(8)
B	0	0	0.3518(8)	0.86(16)
C	$\frac{1}{2}$	$\frac{1}{2}$	0	0.91(19)

$LaIr_2B_2C$

Space group *I4/mmm*, $a = 3.8965(10)$ Å, $c = 10.454(3)$ Å, $Z = 2$, $R = 0.028$, $R_w = 0.033$ (397 independent reflections, 397 observed ($I > 2.5\ \sigma(I)$), 11 parameters

	x	y	z	B_{iso} (Å^2)
La	0	0	0	0.517(13)
Ir	$\frac{1}{2}$	0	$\frac{1}{4}$	0.310(7)
B	0	0	0.3501(23)	1.1(4)
C	$\frac{1}{2}$	$\frac{1}{2}$	0	1.1(3)

3. Results

The $LuNi_2B_2C$-type structure readily accepts other rare earth ions, from the small lutetium up to the large lanthanum ion. The scandium analog can also be made, albeit not in phase-pure form [8]. A regular lanthanide contraction of the crystallographic cell parameters according to Vegard's law is expected. This is indeed observed; however, the tetragonal *c*-axis behaves in an opposite manner to the *a*-axis. The *c*-axis shows an expansion while going from the large ions to the small ones, the inverse of the behaviour of the *a*-axis, which follows the expected trend. As a result, the overall volume contraction is small, from 142.5 Å^3 for La to 127.6 Å^3 for Lu, only an 11% contraction. In Fig. 1, we show the trends for the *a*- and *c*-axis lattice parameters for the different sizes of the lanthanide atoms [9,10] in $LnNi_2B_2C$. With the exception of cerium, the lattice constants depend linearly on the lanthanide radii. The deviation from this dependence for cerium indicates an intermediate or mixed valence state of approximately $Ce^{+3.75}$, revealing hybridization of the Ce 4f orbital with the broader electronic bands from the remainder of the structure.

A linear regression for the a_{tet} and c_{tet} lattice parameters was also derived based on the rare earth atomic radius r_{Ln}, given by Iandelli and Palenzona [9]. For the a_{tet} axis, the function is given by $a_{tet,\,Ln} = 1.5056 \times r_{Ln} + 2.182$ and $c_{tet,\,Ln} = -3.85149 \times r_{Ln} + 13.978$. These fits are shown in Fig. 1 as thin lines.

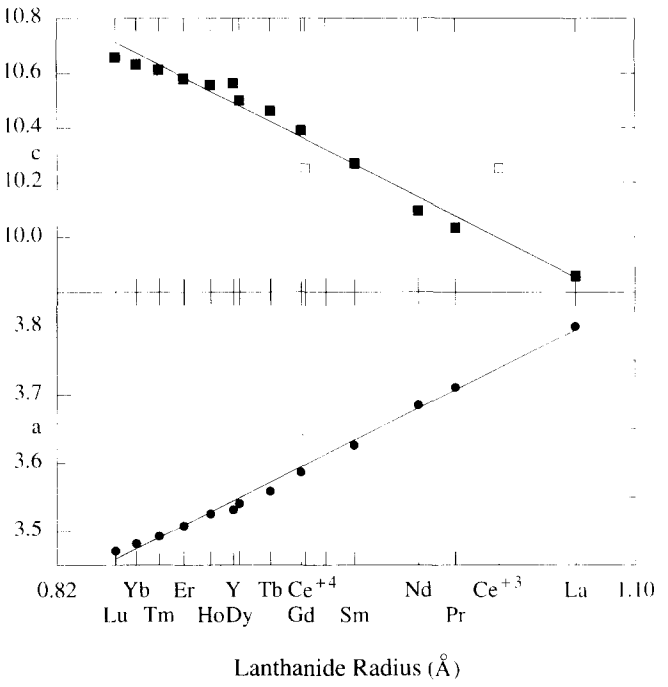

Fig. 1. Tetragonal lattice constants a and c for $LnNi_2B_2C$ with Ln = La, Ce, Sm, Tb, Dy, Y, Ho, Er, Tm, Lu. The radii for Ce^{+3} and Ce^{+4} are both indicated. The solid lines are linear regression fits.

The linear relation for $c_{tet,Ln}$ is a good first-order description: the true behaviour is somewhat 'S' shaped. In order to compare the different lanthanide phases, we are using the lattice parameters derived from the X-ray powder data even where single crystal data are available. Powder lattice parameters are given in Table 2, whereas the lattice parameters obtained from single crystals are given in Table 1, together with the structural data. To remain consistent within the experimental methods, only the single-crystal data for the boron z parameters was used to infer the z(B) parameter for the whole series. All subsequent calculations were then carried out with the lattice parameter data obtained from powders. The single-crystal data, including the lattice parameters, are of a higher precision, but were not used in Table 2.

All the lanthanides follow this given trend well, with the exception of YNi_2B_2C, where the c_{tet} axis is slightly larger than expected. It may be that the difference for the yttrium compound is due to the absence of a partially filled f-shell, since the lanthanides with a similar radius are holmium and dysprosium. The difference, however, is small; the radius for yttrium derived from the a_{tet} axis is 0.897 Å and from the c_{tet} axis 0.886 Å. This would move the yttrium towards the smaller erbium.

The observed behaviour, showing a contraction in one direction, but an expansion perpendicular to it, is intriguing. To study the internal rearrangement of the atoms for the various lanthanides, we carried out full structure refinements for the two end members of the series as well as one representative from the middle of the series, $GdNi_2B_2C$. The atomic positions are constrained by symmetry to be fixed for all atoms except for the z-parameter of the boron atom. The refined z-parameters for boron are La, 0.3492(7), Gd, 0.3569(12) and Lu 0.3621(8). A linear interpolation then allows us to obtain the z-parameter for all the phases in the $LnNi_2B_2C$ series. The linear function has the form $z = -0.05785 \times r_{Ln} + 0.41116$. Results are given in Table 1.

Table 2
Radii, lattice parameters, and z-parameter of boron for $LnNi_2B_2C$

Ln	r	a_{tet}	c_{tet}	z(B)	d(B–C)	d(Ni–B)	α(B–Ni–B)
La[a]	1.071	3.801	9.861	0.3492	1.487	2.137	102.1
Ce^{3+}		3.645	10.251				
Pr	1.013	3.712	10.036	0.3526	1.479	2.123	103.6
Nd	0.995	3.686	10.097	0.3536	1.478	2.119	104.1
Sm	0.964	3.627	10.270	0.3554	1.485	2.112	105.2
Eu[b]	0.950	3.612	10.319	0.3562	1.484	2.112	105.6
Gd[a]	0.938	3.588	10.392	0.3569	1.487	2.110	106.1
Tb	0.923	3.560	10.463	0.3578	1.488	2.107	106.7
Dy	0.908	3.542	10.501	0.3586	1.485	2.106	107.0
Y	0.905	3.533	10.566	0.3588	1.492	2.108	107.3
Ho	0.894	3.527	10.560	0.3594	1.485	2.108	107.5
Er	0.881	3.509	10.582	0.3602	1.479	2.107	107.8
Tm	0.869	3.494	10.613	0.3609	1.476	2.106	108.2
Yb	0.858	3.483	10.633	0.3615	1.473	2.107	108.5
Lu[a]	0.848	3.472	10.658	0.3618	1.473	2.106	108.7

The boron–carbon distance is calculated from the derived z-parameter of boron and the lattice parameters derived from powder data.
[a]Single crystal data for the boron z-parameter.
[b]All crystallographic parameters for Eu^{3+} are calculated.
Estimated standard deviations are: 0.001 Å for a_{tet}, 0.003 Å for c_{tet}, 0.010 for z(B), 0.010 Å for d(B–C), 0.010 Å for d(Ni–B) and 0.50° for α(B–Ni–B).

With the z-parameter known, the boron–carbon distance can be calculated across the whole series. This distance changes less than 0.025 Å, from La to Lu, which indicates a remarkably rigid B–C–B linear structural unit.

From other LnT_2B_2C series, we have studied the starting members, LaT_2B_2C, with T = Rh, Ir and Pt, where small crystals were available to carry out full structure determinations. The smaller lanthanides are less stable for these transition metals, and it is difficult to obtain suitable single crystals.

4. Discussion

The structure of the intermetallic LnT_2B_2C (see Fig. 2) is closely related to the $ThCr_2Si_2$-type structure. The boron–nickel (transition metal) framework is modified by the addition of a carbon atom between two boron atoms bridging the plane of the lanthanide. This linear structural element comprising the three atoms, boron–carbon–boron, is very rigid, and it is aligned along the c-axis. Varying the lanthanide atom in the structure in effect applies a chemical pressure on this subunit. Since the boron–carbon distance does not allow large variation, there is now a part of the structure that cannot adjust to the chemical pressure in a uniform fashion. The alignment of the boron–carbon–boron unit along the c-axis will therefore give a pronounced uniaxial response of the structure to the chemical pressure.

The new $LuNi_2B_2C$-type structure (Fig. 2) can be regarded as a chemically layered structure, with distinct structural units. The structure consists of basically two types of layers, the inverse PbO-type Ni_2B_2 layer and the NaCl-type LnC layer. In the Ni_2B_2 layer the nickel is tetrahedrally coordinated by four boron atoms, at a distance of 2.1 Å. The tetrahedra all share edges, resulting in rather short nickel–nickel distances of 2.45 Å. It is quite remarkable that the Ni–B distance is almost constant, changing only from 2.133 Å for La to 2.102 Å for Lu. The second layer is formed by the lanthanide and carbon atoms, to form a NaCl-type layer. Each lanthanide atom is therefore in a square planar coordination by four carbon atoms and vice versa. The two layers connect via the carbon atoms, defining the above-mentioned linear boron–carbon–boron unit. This is quite reminiscent of the layered high T_c oxide superconductor $LnBa_2Cu_3O_7$, where the CuO_2–Ln–CuO_2 layers are connected via CuO_4 units [11]. Because the rigid connection of the Ni_2B_2 layers does not allow a large variation of the layer spacing, the chemical pressure has to be taken up within the layer itself. The radius variation of the lanthanide will therefore affect the Ln–C distance within the NaCl-type plane, but not the boron–carbon distance. The a_{tet} axis changes from 3.794 Å for La to 3.464 Å for Lu, directly reflecting the Ln–C distance, which is $a_{tet}/\sqrt{2}$. This variation now has a profound effect on the Ni_2B_2 layer. Since the nickel–boron distance can be regarded as constant, the only way for the layer to adjust is by changing the B–Ni–B tetrahedral angle: from 102° for La to 106° for Gd to 108.8° for Lu. This analysis shows that the lutetium compound is much less strained than the lanthanum compound, where the tetrahedral angle deviates substantially from the ideal value of 109.47°. The reduction of the tetrahedral angle now imparts an overall reduction of the Ni_2B_2 layer thickness. This trend is nicely followed: we find Ni_2B_2 layer thicknesses of 1.948 Å for La, 2.215 Å for Gd, and 2.384 Å for Lu. The difference in thickness in the Ni_2B_2 layers in the La and Lu analogs is 0.434 Å, accounting for the overall change of 0.8 Å of the c_{tet} axis. However, nickel–nickel interactions within the Ni_2B_2 layers, due to the decreasing Ni–Ni distance, will eventually modify this simple picture.

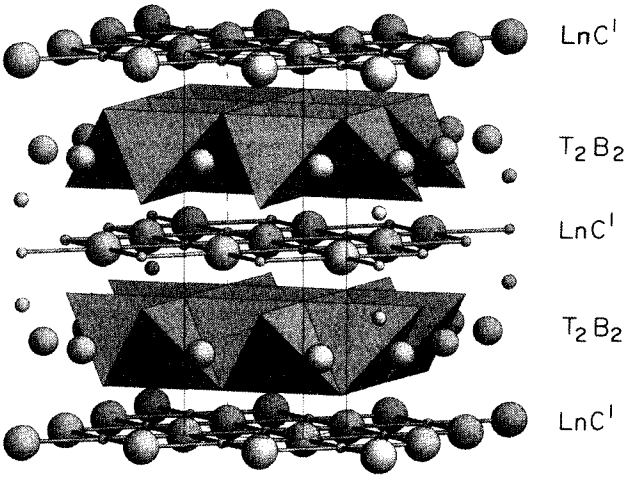

Fig. 2. View of the crystal structures of $LuNi_2B_2C$. The Ni–B framework is indicated by edge-sharing tetrahedra.

The lattice parameters of $CeNi_2B_2C$ do not fit the derived linear relationship as do the other lanthanides. Neither the trivalent nor the tetravalent radius for Ce falls on the line. The approximate valence $Ce^{+3.75}$ obtained by interpolation reveals possible mixed or intermediate valence behaviour of cerium.

To explore the stability range of this new structure type, other transition elements were substituted for nickel. We were successful in obtaining $LnPt_2B_2C$, $LnPt_{1.7}Au_{0.3}B_2C$ [12], $LaRh_2B_2C$ and $LaIr_2B_2C$ [8]. With the exception of the gold-substituted platinum series, we obtained single crystals for all of them, and the data are given in Table 1.

The isoelectronic substitution of platinum for nickel produces a large change in the c_{tet} axis, but only a small change in the a_{tet} axis. Again, the boron–carbon distance is very close to the values for the nickel system, 1.48 Å. However, the Pt_2B_2 layer is thicker, with a

B–Pt–B angle of 106° and a thickness of 2.392 Å. Also, as expected, the Pt–B distance of 2.27 Å is slightly larger than in the Ni–B distance of 2.133 Å. Platinum-containing phases with the smaller lanthanides have not yet been obtained, but it is expected that the B–Pt–B tetrahedral angle will be larger than the ideal angle, producing a further expansion of the layer thickness: there will be a limit imposed by the minimum Pt–Pt distance that the layer will tolerate.

Non-isoelectronic substitutions were carried out by partially substituting the gold for platinum in the $LnPt_{1.7}Au_{0.3}B_2C$ series, with Ln = La, Ce, Pr and Nd. A similar trend of the lattice constants is observed, with the lattice parameters for the cerium compound, again indicating possible mixed or intermediate valence behaviour [12].

The two phases $LaRh_2B_2C$ and $LaIr_2B_2C$ formed, and could be structurally analyzed. There, the valence electron count is reduced by two electrons per formula unit, and the phases are not superconducting above 4.2 K. Only small differences are observed for the two phases. Their lattice parameters are very similar, and therefore, only small differences are expected for the structural parameters. In fact, the transition metal–boron distances are close, 2.213 Å for Rh and 2.274 Å for Pt, the B–T–B angles are 103° for Rh and 102° for Ir, and the boron–carbon distances are almost the same, 1.518 Å for Rh and 1.57 Å for Ir. The T_2B_2 layers are therefore strained. Introducing smaller lanthanides is expected to reduce the strain, but so far, no single-phase material has been obtained.

It is interesting to note that superconductivity is only observed for the smaller lanthanides in the $LnNi_2B_2C$ series [3]. Electronic band structure calculations do reveal a significantly lower density of states for Ln = La than Ln = Lu, but the non-superconducting nature of $LaNi_2B_2C$ is still enigmatic [13, 14]. Since the electrons at the Fermi level are predominantly Ni 3d electrons, the straining of the Ni_2B_2 layer may strongly influence the superconducting behaviour. Since the highest T_c has been observed in the $LuNi_2B_2C$ where the Ni_2B_2 layers are the least strained (and furthest apart), the B–Ni–B angle may serve as an indicator for possible superconductivity. The smallest lanthanide no longer superconducting is dysprosium, with a calculated B–Ni–B angle of 107°, whereas $LaPt_2B_2C$ with a B–Pt–B angle of 106° is a superconductor. Further examinations of other superconducting phases in the LnT_2B_2C system are needed to establish a positive correlation.

5. Summary

The new $LnNi_2B_2$-type structure has been investigated for different lanthanide ions. The structure can be regarded as a layered system, with a 'hard' and a 'soft' layer, accommodating the strain produced by the different sizes of the lanthanides. The Ni_2B_2 layer serves as a cushion, allowing the structure to form with La as well as with Lu. A geometric model based on conservation of boron–carbon and Ni–B bond lengths across the series explains the difference in the behaviour of the tetragonal lattice constants: an expansion for the c_{tet} axis for decreasing lanthanide sizes, and the a_{tet} axis showing the expected decrease.

References

[1] R.J. Cava, H. Takagi, B. Batlogg, H. Zandbergen, J.J. Krajewski, W.F. Peck Jr., R.B. van Dover, R.J. Felder, T. Siegrist, K. Mizuhashi, J.O. Lee, H. Eisaki, S.A. Carter and S. Uchida, *Nature, 367* (1994) 146.

[2] R. Flückiger, in J. Evetts (ed.), *Concise Encyclopedia of Magnetic and Superconducting Materials*, Pergamon, Oxford, 1992, pp. 1–15.

[3] R.J. Cava, H. Takagi, H.W. Zandbergen, J.J. Krajewski, W.F. Peck Jr., T. Siegrist, B. Batlogg, R.B. van Dover, R.J. Felder, K. Mizuhashi, J.O. Lee, H. Eisaki and S. Uchida, *Nature, 367* (1994) 252–253.

[4] R.J. Cava, B. Batlogg, T. Siegrist, J.J. Krajewski, W.F. Peck Jr., S. Carter, R.J. Felder, H. Takagi and R.B. van Dover, *Phys. Rev., B49* (1994) 12, 384–12, 387.

[5] T. Siegrist, H.W. Zandbergen, R.J. Cava, J.J. Krajewski and W.F. Peck Jr., *Nature, 367* (1994) 254–255.

[6] Y. LePage, P.S. White and E.J. Gabe, *Proc. Am. Crystallogr. Assoc. Annual Meeting, Hamilton, Canada, 1986*, AIP, New York, 1986, Poster PA23.

[7] E.J. Gabe, Y. LePage, J.-P. Charland, F.L. Lee and P.S. White, *J. Appl. Crystallogr., 22* (1989) 348–387.

[8] R.J. Cava, J.J. Krajewski and W.F. Peck Jr., unpublished.

[9] A. Iandelli and A. Palenzona, in K.A. Gschneidner and L. Eyring (eds.), *Handbook on the Physics and Chemistry of Rare Earths*, Vol. 2, North-Holland, Amsterdam, 1984, Ch. 13.

[10] R.D. Shannon and C.T. Prewitt, *Acta Crystallogr., B26* (1970) 1046–1048.

[11] Y. LePage, T. Siegrist, W.R. McKinnon, S.A. Sunshine, J.M. Tarascon, L.F. Schneemeyer, G.W. Hull, D.W. Murphy, L.H. Greene, S.M. Zahurak and J.V. Waszczak, *Phys. Rev. B, 36* (1987) 3617.

[12] R.J. Cava, B. Batlogg, J.J. Krajewski, W.F. Peck Jr., T. Siegrist, R.M. Fleming, S. Carter, H. Takagi, R.J. Felder, R.B. van Dover and L.W. Rupp Jr., *Physica C, 226* (1994) 170–174.

[13] L.F. Mattheiss, *Phys. Rev. B, 49* (accepted).

[14] L.F. Mattheiss, private communication.